JCTC Journal of Chemical Theory and Computation

Article

pubs.acs.org/JCTC

Dual Approach to Vibrational Spectra in Solution: Microscopic Influence of Hydrogen Bonding to the State of Motion of Glycine in Water

Yukichi Kitamura,[†,‡] Norio Takenaka,[†,§] Yoshiyuki Koyano,[†] and Masataka Nagaoka*[,†,§,∥]

[†]Graduate School of Information Science, Nagoya University, Furo-cho, Chikusa-ku, Nagoya 464-8601, Japan

[‡]Japan Society for the Promotion of Science (JSPS), Tokyo 102-0083, Japan

[§]Elements Strategy Initiative for Catalysts and Batteries (ESICB), Kyoto University Katsura, Kyoto 615-8520, Japan

[∥]Core Research for Evolutional Science and Technology, Japan Science and Technology Agency, Honmachi, Kawaguchi 332-0012, Japan

Supporting Information

ABSTRACT: We have proposed a new theoretical methodology to clarify the microscopic nature of the vibrational properties in solution, which consists of a combination of the vibrational frequency analyses (VFAs) with two kinds of Hessian matrices, that is, the effective Hessian on the free energy surface (free energy Hessian: "FE-Hessian") and the instantaneous one (instantaneous normal mode Hessian: "INM-Hessian") within QM/MM framework. In these VFAs, the Hessians were obtained by the analytical approach, having the advantages from the aspect of both the computational efficiency and accuracy in comparison to those obtained by the numerical one. In the present study, we have applied them to the glycine aqueous solution. First, by using the VFA with the FE-Hessian (VFA-FEH), we estimated the vibrational frequency shifts induced by solvent water molecules. The calculated values were quantitatively in agreement with experimental ones. It was clearly demonstrated that such vibrational shifts are attributed to not only the structural relaxation but also the explicit solute−solvent interactions (i.e., interatomic interactions). Second, by using the VFA with the INM-Hessian (VFA-INMH), the vibrational spectra in solution were investigated through the vibrational INM densities of states (DOS). By the comparison between the spectroscopic features and the microscopic solvation structure around glycine molecule, it was found that the frequency shifts and bandwidths in IR spectra are closely correlated with the hydrogen bonding (HB) network formations. In particular, the instantaneous changes of vibrational states of the hydroxyl group and carbonyl one, showing apparently inverse tendency on the strength of the HB interaction, can be explained very well on the basis of two different mechanisms, that is, the direct change of electron density in the bonding orbitals and the indirect one due to hyperconjugation between the lone electron pair and the antibonding orbitals, respectively. In conclusion, the present dual VFA approach is a quite useful strategy to interpret the microscopic origin of the experimental vibrational spectra.

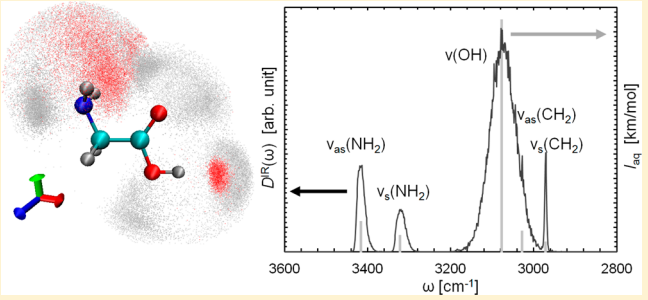

1. INTRODUCTION

Vibrational spectroscopy is one of the most widely used experimental techniques for determining molecular structures, for the identification and characterization of molecules, and for monitoring the chemical reaction processes.[1−3] In general, because the infrared (IR) and Raman peaks are often overlapped due to the spectral line broadening, it is difficult to assign peaks in spectra to particular vibrational modes based on such vibrational spectra. On the other hand, from the theoretical viewpoint, all normal modes and their frequencies of a certain molecule can be automatically obtained by the vibrational frequency analysis (VFA). In fact, the VFA has been generally utilized as the reliable tools for the identification of the experimental spectra in gas phase.[4,5] However, it is still difficult to obtain theoretically such information on the vibrational motions of the chemical species in condensed phase, because of the solvent-induced vibrational coupling by the solute−solvent interactions and their complicated correlations between the vibrational motions.

Until now, a number of theoretical methods have been developed to take solvent effects into consideration. Among them, the dielectric continuum models (DCMs), which are such methods that replace the solvent molecules around the solute by a dielectric continuum,[6] are often used in the cases of requiring highly accurate QM calculation with relatively low calculation cost. However, they have several problems due to the neglect of direct intermolecular interactions such as the hydrogen bonds (HBs) between solutes and solvent molecules.[7−9] On the contrary, the quantum mechanical/molecular

Received: March 19, 2014
Published: July 10, 2014

   dx.doi.org/10.1021/ct500235a | J. Chem. Theory Comput. 2014, 10, 3369−3379

mechanical (QM/MM) method[10] is often utilized as a useful alternative method that only the reactive parts in the whole solution system are treated quantum mechanically while the other part is molecular mechanically. The molecular dynamics (MD) method combined with the QM/MM method (QM/MM-MD method),[11] therefore, can consider legitimately solute−solvent interactions explicitly for instantaneous structural rearrangements of the surrounding solvent molecules.

Under the circumstances, the free energy gradient (FEG) method[12−19] combined with the QM/MM-MD method has been proposed as the structure optimization method on a multidimensional free energy surface (FES) to obtain stable states (SS) and transition states (TS) in condensed phase. In this method, the effective equilibrium structures in solution are obtained as such a molecular structure satisfied with the zero-force condition on the FES, which is analogous to the traditional method on the Born−Oppenheimer potential energy surface (PES) using ab initio molecular orbital (MO) calculation. As with the FEG force, since the Hessian on the FES is similarly obtained, the VFA with FE-Hessian (VFA-FEH) can be executed to obtain both effective normal modes and their vibrational frequencies in solution through the diagonalization of the mass-weighted Hessian matrix on the FES (FE-Hessian). Namely, we can obtain the vibrational frequencies taking into consideration microscopic solute−solvent interaction and thermal fluctuation of the condensed environment by such VFA combined with the QM/MM-MD method. In addition, this method has such an advantage that vibrational frequencies and their fluctuations can be systematically obtained without preparing the empirical vibrational Hamiltonian[20−22] so as to reproduce the vibrational frequencies.

On the other hand, the instantaneous normal mode (INM) analysis[23−26] has been proposed to obtain the approximate vibrational spectra through the diagonalization of the Hessian matrix at each instantaneous configuration of the solute molecule (INM-Hessian). The INM spectra are defined by an ensemble-average of instantaneous $3N$ normal mode eigenvalues over their distribution. By combining it with the QM/MM-MD method, the VFA with the INM-Hessian (VFA-INMH) provides the complementary information that cannot be obtained by VFA-FEH approach. While the latter approach provides a set of effective normal modes and their vibrational frequencies in solution, the former does an instantaneously decoupled second-order description of the vibrational motions of solute molecule along the time-dependent trajectory. Accordingly, the VFA-INMH approach is very useful to clarify the "instantaneous" solvent effects, determining a number of instantaneous vibrational frequencies and vectors.

In this study, we have proposed a new theoretical methodology employing both the VFA-FEH and the VFA-INMH approaches within the QM/MM framework. In our previous study,[16,17] the QM/MM Hessians have been estimated numerically, requiring a lot of calculation times. However, to reduce these calculation costs, they are estimated in the present study by evaluating new analytically derived expressions of the vdW components in QM/MM Hessian. For a preliminary application using the present dual VFA approach, the vibrational spectra of H_2O molecule in liquid water have been reported.[19] Then, we have explained the dual VFA approach clearly and applied it to the neutral form of glycine molecule in aqueous solution, which is still a good target of studies for its pivotal biochemical importance.[9,27] Further, we have investigated the microscopic origin of vibrational frequency shifts and vibrational spectra of the glycine molecule in aqueous solution.

In this article, we explain the methodology for the VFAs in solution in section 2. In the results and discussion in section 3, we first discuss the computational efficiency and accuracy of the present VFA employing the analytical QM/MM Hessian in section 3.1. Next, in section 3.2, we show that the calculated vibrational frequency shifts by the VFA-FEH approach are in quite good agreement with the experimental ones. To estimate the importance of the explicit solvent effect, we have also shown comparatively the calculation results by the VFA with the CPCM-Hessian (VFA-CPCM) via the conductor-like polarizable continuum model (CPCM) method. As a result, it was found that the vibrational shifts are attributed to not only the structural relaxation but also the explicit solute−solvent interactions. Finally, by using the VFA-INM approach, we have investigated the approximate IR spectra in aqueous solution considering together the densities of states (DOS) of the vibrational INMs. By comparing the spectroscopic features with the solvation structure around glycine molecule, it was clearly recognized that the IR spectra are influenced by the hydrogen bond (HB) formation between the solute molecule and the first hydration water molecules. Furthermore, by the natural bond orbital (NBO) analysis, the instantaneous vibrational spectral shift of the hydroxyl group and that of the carbonyl one can be differently explained on the basis of two different effects, that is, the electron density effect in the bonding MO and the hyperconjugation effect between the MOs of the lone electron pair and the antibonding MO, respectively. Finally, the concluding remarks are provided in section 4.

2. THEORY AND COMPUTATIONAL METHODS

2.1. Analytical Hessian in the QM/MM Formalism. In the QM/MM treatment of reactive solute molecules in solution, only the reactive parts in the whole solution system are usually treated quantum mechanically, while the other parts are molecular mechanically. The total system potential energy V is obtained by

$$V = \langle \Psi | \hat{H}_{QM} + \hat{H}_{QM/MM} | \Psi \rangle + V_{MM} \quad (1a)$$

$$= \langle \Psi | \hat{H}_{QM} + \hat{H}^{est}_{QM/MM} | \Psi \rangle + \hat{H}^{vdW}_{QM/MM} + V_{MM} \quad (1b)$$

$$= V_{SB} + V_{MM} \quad (1c)$$

where $\hat{H}_{QM}$ stands for the standard Hamiltonian of the QM systems and $\hat{H}_{QM/MM}$ denotes the interaction between the QM and the MM system. The electrostatic (est) interaction of the polarized QM density with an external charge distribution (e.g., a set of MM point charges) is estimated by the electrostatic embedding scheme, which is implemented by adding the contribution of the MM point charges to the 1-electron Hamiltonian ($\hat{H}^{est}_{QM/MM}$ in eq S4 in the Supporting Information), while the van der Waals (vdW) interaction is typically described by a Lennard−Jones potential ($\hat{H}^{vdW}_{QM/MM}$ in eq S5 in the Supporting Information). Here, V_{SB} denotes the sum of both the potential energy of the solute and the interaction energy between the solute and solvent molecules.

The Hessian $\mathbf{H}$ in the QM/MM method, which is a $3N \times 3N$ matrix containing all the second order derivatives of the potential energy V with respect to the mass-weighted (mw) solute's Cartesian coordinates $\mathbf{q}^s_{mw}$, can be expressed as follows,

$$\mathbf{H} = \frac{\partial^2 V_{SB}(\mathbf{q}^s)}{\partial \mathbf{q}^s_{mw} \partial \mathbf{q}^s_{mw}} = \left[\left\{ \frac{\partial^2 \langle \Psi | \hat{H}_{QM} + \hat{H}^{est}_{QM/MM} | \Psi \rangle}{\partial q_{\alpha A} \partial q_{\beta B}} \right\} + \left\{ \frac{\partial^2 \hat{H}^{vdW}_{QM/MM}}{\partial q_{\alpha A} \partial q_{\beta B}} \right\} \right] \tag{2a}$$

with

$$\mathbf{q}^s_{mw} = \{q_{\alpha A}\} = \{\sqrt{m_1}x_1, \sqrt{m_1}y_1, \sqrt{m_1}z_1, \cdots, \sqrt{m_A}\alpha_A, \cdots, \sqrt{m_N}x_N, \sqrt{m_N}y_N, \sqrt{m_N}z_N\} \tag{2b}$$

where subscripts A and B are the indices of the QM atoms (which have a value from 1 to N), and α and β denote the x, y, and z components, and m_A is the mass of the A-th QM atom. The Hessian $\mathbf{H}$ consists of the components originating in the est and the vdW contribution. The est components are analytically computed by the program GAUSSIAN,[28] where approximate methods of electronic state calculations are available, for example, the Hartree−Fock (HF), second-order Møller−Plesset perturbation theory (MP2), configuration interaction with singles (CIS), complete active space self-consistent field (CASSCF) method, and all the density functional theory (DFT) methods. On the other hand, since the vdW components are expressed as such analytical functions of those coordinate variables on the same atom ($A = B$) as follows,

$$\frac{\partial^2 \hat{H}^{vdW}_{QM/MM}}{\partial q_{\alpha A} \partial q_{\beta A}} = \begin{cases} \sum_M \varepsilon_{AM} \left[24 \left(7 \left(\frac{r_{AM}}{R_{AM}} \right)^{12} - 4 \left(\frac{r_{AM}}{R_{AM}} \right)^{6} \right) \frac{(q_{\alpha A} - q_{\alpha M})^2}{R^4_{AM}} \right. \\ \left. -12 \left(\left(\frac{r_{AM}}{R_{AM}} \right)^{12} - \left(\frac{r_{AM}}{R_{AM}} \right)^{6} \right) \frac{1}{R^2_{AM}} \right] \quad (\alpha = \beta) \\ \sum_M \varepsilon_{AM} \left[24 \left(7 \left(\frac{r_{AM}}{R_{AM}} \right)^{12} - 4 \left(\frac{r_{AM}}{R_{AM}} \right)^{6} \right) \right. \\ \left. \times \frac{(q_{\alpha A} - q_{\alpha M})(q_{\beta A} - q_{\beta M})}{R^4_{AM}} \right] \quad (\alpha \neq \beta) \end{cases} \tag{2c}$$

where M denotes an integral number discriminating the MM atoms, and ε_{AM} and r_{AM} are a couple of LJ parameters for the A-th QM atom interacting with the M-th MM atom, and R_{AM} is the distance between the A-th QM atom and the M-th MM one. In the case of glycine molecule ($N = 10$), only 90 components remain as the nonzero elements in the Hessian matrix.

2.2. Vibrational Frequency Analysis (VFA) in Solution.

2.2.1. Effective Normal Modes of Vibration and Vibrational Frequencies Using FE-Hessian: VFA-FEH Analysis. In order to obtain the effective normal modes $\{Q_i\}$ and their vibrational frequencies $\{\omega_i\}$ in solution, we have proposed the VFA using the Hessian on the FES ("FE-Hessian"), that is, the VFA-FEH analysis. In this analysis, all the molecular vibrations are described under the harmonic approximation on the FES. Then, the FE-Hessian $\mathbf{H}^{FE}$ can be analytically expressed as follows,[12]

$$\mathbf{H}^{FE}(\mathbf{q}^s) = \frac{\partial^2 A(\mathbf{q}^s)}{\partial \mathbf{q}^s_{mw} \partial q^s_{mw}} = \left\langle \frac{\partial^2 V_{SB}(\mathbf{q}^s)}{\partial \mathbf{q}^s_{mw} \partial \mathbf{q}^s_{mw}} \right\rangle - \frac{1}{k_B T} \left[\left\langle \frac{\partial V_{SB}(\mathbf{q}^s)}{\partial \mathbf{q}^s_{mw}} \frac{\partial V_{SB}(\mathbf{q}^s)^T}{\partial \mathbf{q}^s_{mw}} \right\rangle - \left\langle \frac{\partial V_{SB}(\mathbf{q}^s)}{\partial \mathbf{q}^s_{mw}} \right\rangle \left\langle \frac{\partial V_{SB}(\mathbf{q}^s)}{\partial \mathbf{q}^s_{mw}} \right\rangle^T \right] \tag{3}$$

where the brackets $\langle \cdots \rangle$ denote the time average that is equal to the equilibrium ensemble average and the superscript T denotes the transposition. Since the contribution of the second term of the force fluctuation in eq 3 was considered small enough in comparison with that of the first term,[16−18] the approximation to neglect the second term in eq 3 was adopted in present study,

$$\frac{\partial^2 A(\mathbf{q}^s)}{\partial \mathbf{q}^s_{mw} \partial \mathbf{q}^s_{mw}} \approx \left\langle \frac{\partial^2 V_{SB}(\mathbf{q}^s)}{\partial \mathbf{q}^s_{mw} \partial \mathbf{q}^s_{mw}} \right\rangle \tag{4}$$

Thereby, FE-Hessian matrix $\mathbf{H}^{FE}$ is analytically obtained as an equilibrium ensemble average of the instantaneous Hessian matrix $\mathbf{H}$ in solution.

The effective vibrational frequencies $\{\omega_i\}$ are estimated by diagonalizing of the FE-Hessian matrix $\mathbf{H}^{FE}$,

$$\mathbf{U}^{-1}\mathbf{H}^{FE}\mathbf{U} = \mathbf{K}\mathbf{I} = \{k_i\}\mathbf{I} \tag{5a}$$

and

$$\omega_i = \frac{1}{2\pi c}\sqrt{k_i} \tag{5b}$$

and

$$\{Q_i\} = \{\sum_{A=1}^{N} \sum_{\alpha}^{x,y,z} u_{i,A\alpha} q_{A\alpha}\} = \mathbf{U}\mathbf{q}^s_{mw} \tag{5c}$$

where $\mathbf{U}$ and $\mathbf{I}$ are $3N$-dimensional unitary and identity matrices, respectively. In eq 5a, $\mathbf{K}$ is a matrix whose diagonal elements consists of a set of the eigenvalues $\{k_i\}$, and c is the speed of light in eq 5b. A set of $3N$ effective normal modes of vibration $\{Q_i\}$ can be also obtained from eigenvectors corresponding to those effective vibrational frequencies ω_i.

2.2.2. Approximate Vibrational Spectra Using INM-Hessian: VFA-INMH Analysis. In order to elucidate the solvation effects on vibrational properties in aqueous environment, we propose another VFA analysis called the VFA-INMH analysis, that is, the VFA with the instantaneous Hessian ("INM-Hessian") combined with the QM/MM-MD method, calculating the approximate vibrational spectra via the instantaneous normal mode (INM) analysis.[23−26] The INMs are defined by diagonalizing the INM-Hessian matrix $\mathbf{H}^{INM}$ at any instantaneous configuration $\mathbf{R}'$, and the eigenvalues $\{k_i^{INM}\}$ are obtained as

$$\{k_i^{INM}\}_{\mathbf{R}'}\mathbf{I} = \mathbf{U}^{-1}_{\mathbf{R}'}\mathbf{H}^{INM}\mathbf{U}_{\mathbf{R}'} \tag{6a}$$

with

$$\mathbf{H}^{INM} = \left. \frac{\partial^2 V_{SB}(\mathbf{q}^s)}{\partial \mathbf{q}^s_{mw} \partial \mathbf{q}^s_{mw}} \right|_{\mathbf{R}'} \tag{6b}$$

and

$$\omega_i^{INM} = \frac{1}{2\pi c}\sqrt{k_i^{INM}} \tag{6c}$$

At a finite temperature, most of instantaneous configurations $\mathbf{R}'$ do not correspond exactly to any local minimum on the PES. Consequently, since the forces are usually nonzero and all the eigenvalues of the INM Hessian matrix are not necessarily non-negative, those normal modes with the negative eigenvalues are called unstable modes.[23,24] They are corresponding to such modes with imaginary frequencies, to show the instantaneous motions on an upside-down potential, and are associated with a

dx.doi.org/10.1021/ct500235a | J. Chem. Theory Comput. 2014, 10, 3369−3379

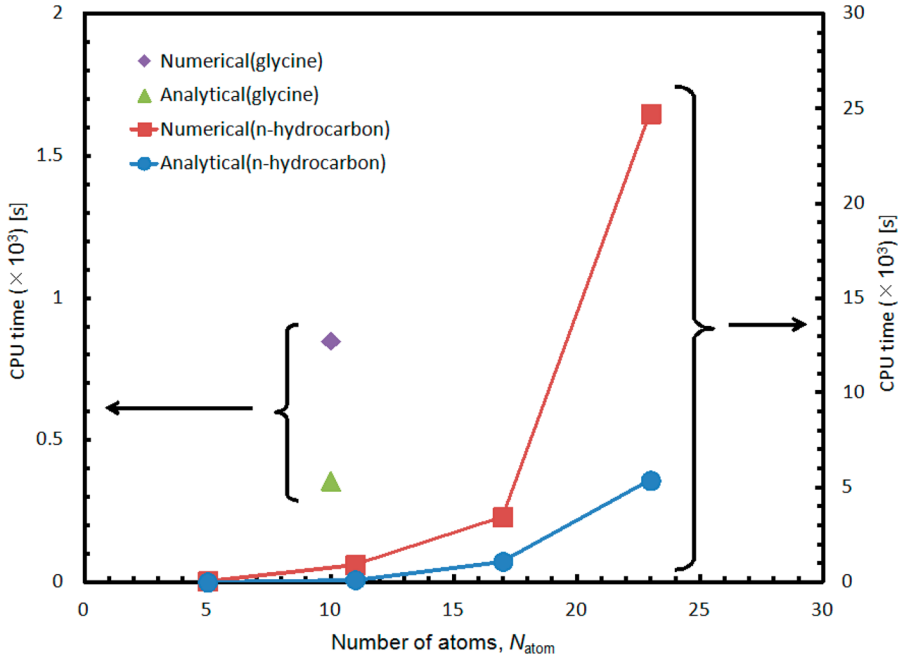

Figure 1. CPU times for *n*-hydrocarbons (C_nH_{2n+2}, n = 1,3,5,7) and glycine molecule. It was obtained by averaging the calculation time for ten configurations. All the calculations were carried out with an Intel Xeon E3-1270 (3.4 GHz) machine. Note that the right and left ordinate axes represent the CPU times for *n*-hydrogens and glycine molecule, respectively.

barrier between two stable wells (e.g., the double wells) or shoulder of a single well.[24−26]

To characterize the ensemble-averaged vibrational frequency distribution, the vibrational INM DOS[23−26] are defined as follows,

$$\rho(\omega) = \left\langle \frac{1}{3N - N_m} \sum_{i=1}^{3N-N_m} \delta(\omega - \omega_i^{INM}) \right\rangle \tag{7}$$

Here, N_m shows the number of normal modes with imaginary frequencies. In addition, to obtain the infrared (IR) spectra, we define the vibrational INM DOS weighted by the dipole moment derivatives $\partial\mu_{\mathbf{R}'}/\partial Q_i^{INM}$, that is, with respect to the corresponding INM coordinates $Q_i^{INM}(= \mathbf{U}_{\mathbf{R}'}\mathbf{q}^s_{mw})$ as follows,

$$D^{IR}(\omega) = \left\langle \frac{1}{3N - N_m} \sum_{i=1}^{3N-N_m} w_i^{IR} \delta(\omega - \omega_i^{INM}) \right\rangle \tag{8a}$$

with

$$w_i^{IR} = \frac{1}{4\pi\varepsilon_0} \frac{N_A \pi}{3c^2} \left(\frac{\partial \mu_{\mathbf{R}'}}{\partial Q_i^{INM}} \right)^2 \tag{8b}$$

where ε_0, N_A, and $\mu_{\mathbf{R}'}$ are vacuum permittivity, Avogadro's number and the net dipole moment at an instantaneous configuration $\mathbf{R}'$, respectively. Actually, we utilize the instantaneous IR intensities calculated with GAUSSIAN09[28] as w_i^{IR}, and the ensemble-averaged IR intensities I_{aq} in solution are estimated as follows,

$$I_{aq}(\omega) = \frac{D^{IR}(\omega)}{\rho(\omega)} = \frac{\left\langle \frac{1}{3N - N_m} \sum_{i=1}^{3N-N_m} w_i^{IR} \delta(\omega - \omega_i^{INM}) \right\rangle}{\left\langle \frac{1}{3N - N_m} \sum_{i=1}^{3N-N_m} \delta(\omega - \omega_i^{INM}) \right\rangle} \tag{9}$$

where $\delta\omega$ is the width of a bin for integration, being set at 1 cm^{-1} in this study. I_{aq} means the absorption coefficient for IR spectra, which is independent of temperature, and has an inherent value with each vibrational mode. Then, $D^{IR}(\omega)$ can be represented by

$$D^{IR}(\omega) = I_{aq}(\omega)\rho(\omega) \tag{10}$$

and therefore, the total spectral line of the approximate IR spectra is contributed by two components, I_{aq} and ρ, while I_{aq} has a significant influence on the peak height. On the other hand, the broadening of spectra only depends on ρ which has the temperature dependence.

The vibrational INM DOS is obtained as the ensemble-averaged value of instantaneous normal modes as a function of vibrational frequency and can provide information on solvent vibrational fluctuations induced by the solvation effects. However, the VFA-INMH analysis cannot necessarily identify any general feature of microscopic vibrational motions in the vibrational spectroscopy because such a normal mode might take an individual different characteristic depending on the instantaneous configuration. On the other hand, in the VFA-FEH analysis, the effective normal modes and their vibrational frequencies at the equilibrium structure in solution are uniquely obtained. Therefore, by using these two kinds of VFAs using FE- and INM-Hessians, we can assign the peaks in the vibrational spectra to the microscopic vibrational motions, and take some insights into the microscopic solvation effects on the spectroscopic line shape.

2.3. Computational Details. The QM/MM-MD simulations were performed for a whole system, which consist of one QM glycine molecule and 759 MM water molecules in a rectangular simulation cell with linear dimensions L_x = 28.56 Å, L_y = 27.95 Å, L_z = 28.93 Å. The simulation cell box was adjusted after executing the classical MM-MD simulation with *NPT* ensemble at 1 atm. For estimation of the effective atomic charges of the solute glycine molecule, we employed the ESP atomic charges obtained by Merz−Kollman scheme.[29,30] Then, the three-dimensional periodic boundary condition was imposed. The temperature was controlled to 300 K by the

dx.doi.org/10.1021/ct500235a | J. Chem. Theory Comput. 2014, 10, 3369−3379

Berendsen algorithm so that the whole system might be maintained to be an *NVT* ensemble. The nonbonded cutoff distance was chosen as 10.0 Å. The leapfrog algorithm was used to integrate a set of simultaneous equations of motion. After equilibration run, we have obtained the equilibrium structure of the glycine molecule in aqueous solution to be the equilibrium structure optimized by the standard FEG method (the details of the optimization procedure are shown in section A.2 of Appendix in the Supporting Information). A set of ten sampling runs for an FEG optimization cycle were executed concurrently each for 50 ps with a time step 1.0 fs. At the optimized structure, for estimating Hessian matrices for the VFAs, we used 50 000 snapshots, which were collected from the total 500 ps MD trajectory with the time interval of 10 fs. To improve the statistics, this 500 ps MD calculation was also executed concurrently with ten independent starting solvent configurations with the optimized glycine structure.

For the purpose to execute the classical MM-MD and ab initio QM/MM-MD simulation, we used the AMBER–GAUSSIAN interface (AG-IF),[31] combining the MD simulation program package AMBER 9.0[32] with the ab initio MO program GAUSSIAN03.[33] In the present study, a solute glycine molecule was taken as a QM part and described at MP2 method with 6-31+G(d,p) basis set. On the other hand, the MM solvent water molecules were taken as the remaining MM part where each water molecule is represented by the rigid TIP3P model.[34]

3. RESULTS AND DISCUSSION

3.1. Computational Efficiency and Accuracy of Analytical Hessian Expressions. First, we show the computational efficiency and accuracy of the present analytical Hessian expressions, where the QM/MM Hessians were obtained by estimating analytically derived formula (eq 2), that is, the analytical VFA approach. In our previous numerical VFA approach,[16,17] the second derivatives of the energies (the numerical Hessians) were obtained by the central difference method using the analytical first derivatives. To discuss the difference of the computational performance between the analytical and the numerical VFA approaches in solution, we have estimated CPU times and numerical errors of the vibrational frequencies, which were calculated by the sequential ten configurations after equilibration. For the benchmark calculations, we have employed a series of *n*-hydrocarbon C_nH_{2n+2} (n = 1,3,5,7) and the glycine molecule in aqueous solution. Here, we have adopted at MP2/6-31+G(d, p) and TIP3P water model in two systems, and the geometries of *n*-hydrocarbon C_nH_{2n+2} were obtained with the equilibrium structures in gas phase, while that of the glycine molecule was optimized by the FEG method.

Figure 1 shows that the CPU times for *n*-hydrocarbon (C_nH_{2n+2}, n = 1,3,5,7) and glycine molecule by the numerical and analytical VFA approaches. As a result, the CPU times by the analytical VFA approach were less than those by the numerical VFA one in any cases, being drastically reduced up to their 15–20%. On the other hand, that of glycine molecule by the analytical VFA approach was reduced to about 40% of the numerical VFA one. This is because we used for glycine more basis functions per atom (cf. $C_2H_5NO_2$, N_{basis} = 120), requiring a high computational cost in the analytical approach, as compared with for *n*-hydrocarbon molecules (cf. C_3H_8, N_{basis} = 97). In other words, such difference about computational efficiency between two systems (i.e., *n*-hydrocarbons and glycine molecule) should be due to the system-size dependence of the analytical and the numerical VFA approach. Nevertheless, it can be said in general that the present analytical VFA approach is very efficient from the aspect of the computational efficiency in comparison with the numerical VFA approach.

With respect to the numerical accuracy, we have shown in Table 1 the numerical errors of vibrational frequencies in two ways, that is, the maximum (MAX) absolute value among all the frequency differences

Table 1. Numerical Errors of Vibrational Frequencies [cm^{-1}] (the Maximum (MAX) Absolute Value among All the Frequency Differences and Their Root Mean of Square (RMS) Value) in Three Different System Sizes, That Is, Methane, Heptane, and Glycine in Solution[a]

	numerical error [cm^{-1}]		system size	
component	MAX[b]	RMS[c]	N_{atom}	N_{basis}
methane	18	8	5	39
glycine	122	29	10	120
heptane	109	22	23	213

[a]The system sizes are denoted by the number of atoms and the degree of basis sets. [b]$MAX = \max\{|\omega_i^{num} - \omega_i^{ana}| i \in \{1, 2, \cdots, 3N-6\}\}$. [c]$RMS = (\sum_{i=1}^{3N-6}(\omega_i^{num} - \omega_i^{ana})^2/(3N-6))^{1/2}$.

$$MAX = \max\{|\omega_i^{num} - \omega_i^{ana}| i \in \{1, 2, \cdots, 3N-6\}\} \quad (11a)$$

and their root-mean-square (RMS) value,

$$RMS = \sqrt{\sum_{i=1}^{3N-6}(\omega_i^{num} - \omega_i^{ana})^2/(3N-6)} \quad (11b)$$

using the exact vibrational frequencies obtained by the analytical VFA approach in three different system sizes, that is, methane, heptane, and glycine molecules in solution.

As for methane molecule in solution, the MAX and the RMS value were 18 and 6 cm^{-1}, respectively. On the other hand, in gas phase, their numerical errors (i.e., MAX and RMS) were 0.3 and 0.1 cm^{-1}, respectively. The errors in solution were considerably large as compared with those in gas phase (<1 cm^{-1}). In previous study,[48,49] it was reported that the average deviations from the experimental values by the MP2 method range from +27 to +92 cm^{-1} in small molecules, that is, H_2N_2, H_2CO, and NH_3, and the numerical errors in solution were not negligible when compared with experimental values. In general, with the increase of the system size, the numerical errors became significantly increased. In addition, it is exceptional that the error of glycine molecule was larger than that of heptane molecule in spite of its smaller molecule size. This can be attributed to the presence of the stronger hydration around a glycine molecule, which increases the solute–solvent contribution in Hessian, bringing about the large numerical errors. Namely, the numerical errors would be highly influenced by difference of the surrounding environment, that is, the microscopic solute–solvent interactions.

3.2. Vibrational Frequency by VFA using FE-Hessian: Importance of Inclusion of Explicit Solvation Effect. Table 2 shows a triple of typical vibrational frequencies (ω_{gas}, ω_{CPCM}, ω_{FE}) of glycine molecule in gas phase and in aqueous solution with their vibrational frequency shifts induced by the solute–solvent interactions ($\Delta\omega_{CPCM}$, $\Delta\omega_{FE}$), which are scaled by the recommended factor of 0.9486.[35] In addition, they were

Table 2. Calculated Vibrational Frequencies[a] ω (cm^{-1}) and Their Shifts from in Gas Phase to in Aqueous Solution $\Delta\omega$ (cm^{-1})

mode	gas phase	in water		frequency shift		
	ω_{gas}	ω_{CPCM}	ω_{FE}	$\Delta\omega_{CPCM}$[b]	$\Delta\omega_{FE}$[c]	$\Delta\omega_{exp}$
			Stretching			
$\nu_{as}(NH_2)$	3476	3351	3416	−125	−60	−13[d]
$\nu_{s}(NH_2)$	3381	3262	3322	−119	−59	
ν(OH)	3570	3047	3077	−523	−493	−320[d]
$\nu_{as}(CH_2)$	3011	2990	3028	−21	+17	
$\nu_{s}(CH_2)$	2958	2936	2972	−22	+14	
ν(CO)	1708	1657	1691	−51	−17	−39[d]
			Bending			
δ(COH)	1241	1232	1338	−9	+97	
δ(COH)+ $\gamma_{s}(NH_2)$	886	897	990	+11	+104	
γ(COH)	606	563	997	−43	+391	+416[e]
$\gamma_{as}(NH_2)$	225	221	505	−4	+280	

[a]Normal vibrational frequencies (in cm^{-1}) scaled by 0.9418 (ref 35). [b]$\Delta\omega_{CPCM} = \omega_{CPCM} - \omega_{gas}$. [c]$\Delta\omega_{FE} = \omega_{FE} - \omega_{gas}$. [d]FTIR data for Gly-$(H_2O)$ and Gly-$(H_2O)_2$ cluster in Ar matrix.[4] [e]FTIR data for Gly-(1-methyluracil) cluster in Ar matrix.[5]

compared with the experimental values $\Delta\omega_{exp}$ obtained by the Fourier transform infrared (FT-IR) spectroscopy measurement of glycine-$(H_2O)_n$ (n = 1,2)[4] and glycine-(1-methyluracil) H-bond complexes.[5] It should be noted that the vibrational frequencies by the FE- and the CPCM-Hessian are calculated at the optimized structures by the FEG and the CPCM method, respectively.

Both $\Delta\omega_{CPCM}$ and $\Delta\omega_{FE}$ for the stretching modes (>1650 cm^{-1}) with the exception of those of CH_2 group were red-shifted, and $\Delta\omega_{FE}$ agreed well with $\Delta\omega_{exp}$ in comparison with $\Delta\omega_{CPCM}$ (see Table 2). On the other hand, for the four bending modes (≤1650 cm^{-1}), ω_{FE} showed the large blue-shifts in solution. According to the previous experimental studies,[36−45] such tendency is reasonable and common in the intermolecular hydrogen bonding (HB) systems. In particular, ω_{FE} of γ(COH) showed the largest blue-shift (+391 cm^{-1}) in the four and was clearly consistent with $\Delta\omega_{exp}$ (+416 cm^{-1}). In contrast to $\Delta\omega_{FE}$, $\Delta\omega_{CPCM}$ for the bending modes was very small in any case, showing that the inclusion of explicit effect of HBs is inevitable to reproduce vibrational frequency shifts for the bending modes. It was understood, therefore, that the present VFA-FEH approach can provide the more reasonable estimations of vibrational frequency shifts induced by the solvent molecules in solution.

In order to clarify the microscopic origin of such vibrational frequency shifts $\Delta\omega_{FE}$, we have investigated two essential effects, that is, the structural relaxation of glycine molecule itself and the explicit solvation structure around it. According to the comparison between the geometries in gas phase and in aqueous solution (see Table S1 in the Supporting Information), the OH bond length in the —OH group (r(O—H)) was found to increase from 0.973 Å in gas phase to 1.005 Å in aqueous solution (FEG method). Similarly, the NH and the CO bond lengths in the —NH_2 and >CO groups (r(N—H) and r(C═O)) increased, although their changes (+0.006 Å and +0.009 Å) were almost negligible in comparison to that of the OH one (+0.032 Å). In relation to the increase of such bond lengths, the stretching-modes were found to show red-shift in aqueous solution (see Table 2). On the other hand, while the CH bond lengths of the >CH_2 group (r(C—H)) are almost unchanged (−0.001 Å), both its symmetric and asymmetric modes showed slight blue-shifts. In addition, all the bond lengths by FEG method show tendency to increase from those in gas phase, except the CH bond lengths, while these bond lengths by CPCM method also increased (+0.001 Å), their relating stretching modes $\nu_{as}(CH_2)$ and $\nu_{s}(CH_2)$ showing red-shift (i.e., $\Delta\omega_{CPCM}$ in Table 2). The changes of CH bond lengths are due to the nonelectrostatic intermolecular interaction with the closest water molecule. It is considered, therefore, that the description of nonelectrostatic interactions by the CPCM method is inadequate for considering these contributions. The $\Delta\omega_{FE}$ for stretching-modes were closely related to the bond length elongation and such tendency also corresponds to the previous experimental results in the various HB systems.[36−45] Thus, it is considered that the mechanism of frequency shifts of the stretching-modes would be attributed to the softening (or hardening) of vibrational frequency modes due to the bond length elongation (or shortening). However, since there is almost no correlation between $\Delta\omega_{FE}$ of the bending-modes (see Table 2) and the bond angles (see Table S1 in the Supporting Information), the large blue-shifts of ω_{FE} of the bending-modes in aqueous solution cannot be explained by only the changes in bond angles of the glycine molecule.

Next, we have shown in Figure 2 the spatial distributions of oxygen (red) and hydrogen (gray) atoms of solvent water molecules in the first hydration shell around the glycine molecule. It can be clearly seen that the maxima of the oxygen atom distribution are located on the extended line of the O—H and N—H bond of glycine molecule (see Figure 2). In addition, the hydrogen atom distributions are also high around the area located on the direction extended from the N atom of —NH_2 group and O atom of >CO group toward their electron lone-pairs of each atom (see Figure S1 in the Supporting Information). It was found that the surrounding water molecules clearly form HBs with the —OH, —NH_2 and >CO groups. In particular, it was suggested that there are several strong HBs between the —OH group and solvent water molecules. For quantitative estimation of the strength of such HBs, Figure 3 shows the relative frequency distributions of HB angles of the four kinds ($\theta_{OH\cdots Ow}$, $\theta_{CO\cdots Hw}$, $\theta_{N\cdots HOw}$, and $\theta_{NH\cdots Ow}$). The $\theta_{OH\cdots Ow}$ shows the clear maximum value at ∼170 deg, with the peak width sharper than those of other three angles. Actually, the time-averaged HB numbers of OH···Ow, CO···Hw, N···HOw, and NH···Ow were estimated to be 1.03, 0.41, 0.28 and 0.58, respectively. The differences among the HB strengths of functional groups can be interpreted due to those among the proton affinities of donor—acceptors,[46] and they are in agreement with the general tendencies in previous studies.[47] It is understood that the magnitudes of vibrational frequency shifts of stretching modes (ν(CO), $\nu_{as}(NH_2)$, ν(OH)) were found to increase in the same order as the HB numbers (see Table 2).

In contrast to the present VFA approach, the CPCM method, a representative DCM (dielectric continuum model), cannot include the explicit solute—solvent interactions such as HBs. According to the comparison between $\Delta\omega_{CPCM}$ with $\Delta\omega_{FE}$ for the bending-modes, such large blue shifts of ω_{FE} in aqueous solution can be understood to be brought about by the microscopic solute—solvent interactions. The mechanism must be explicitly explained by the steric hindrance by the HB water molecules (see Figure 2), which induce the modification of the

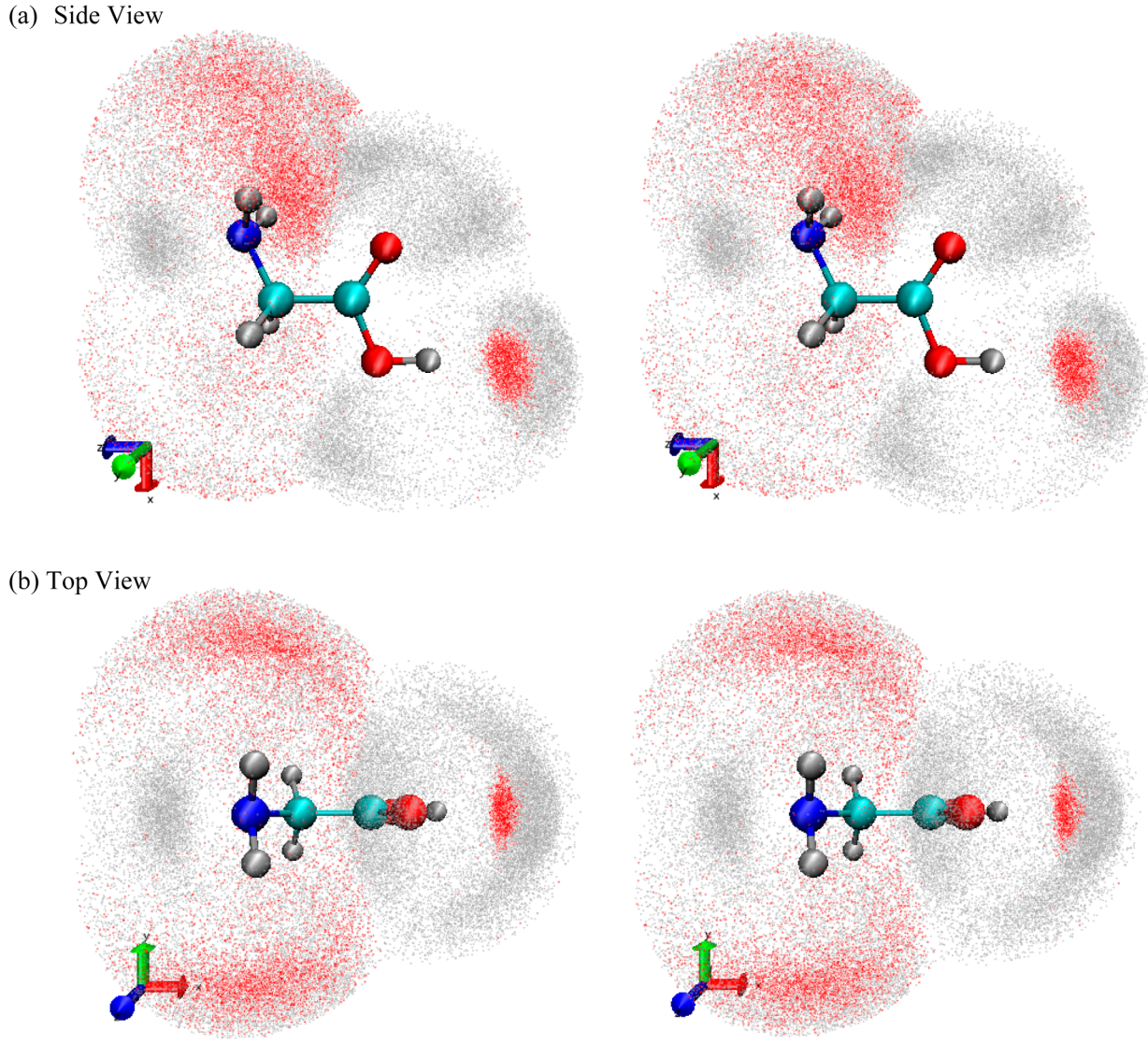

Figure 2. Stereo view of the spatial distribution of oxygen and hydrogen atoms of a water molecule in the first hydration shell around the solute glycine molecule: (a) side view and (b) top view. The red points indicate the oxygen atom of water molecule, and the gray one indicate the hydrogen atom.

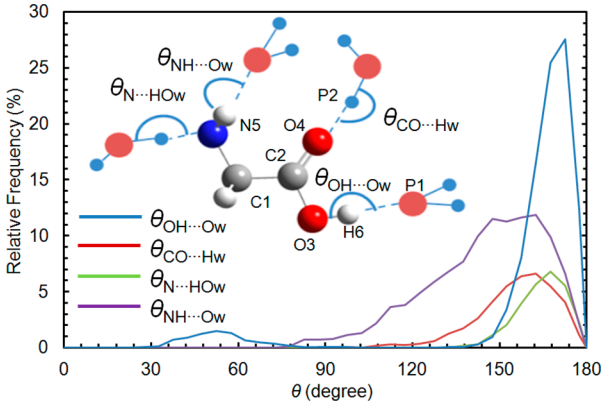

Figure 3. Relative frequency distribution of the hydrogen bond angles.

original PES of the solute and consequently bring about the shifts in the vibrational frequencies. Since the bending motions generally occur oscillatorily orthogonal to the HB direction, the stronger HB formation should make their motions more difficult to occur. As a result, it is considered that the bending-modes including −OH and $-NH_2$ groups show the large blue-shifts in aqueous solution. Moreover, the experimental vibrational shift of Gly-(1-methyluracil) cluster agreed well with our calculated value. This fact supports that their blue-shifts are brought about by a few HB water molecules. From the above comparison with the results by experiment and the CPCM method, it is concluded that the inclusion of explicit solvent effect must be essential to understand even qualitatively the microscopic origin of the experimental vibrational shifts in solution.

3.3. Vibrational Spectra by the VFA-INMH Analysis: Strong Correlation between the Explicit HBs and Vibrational Spectra. In order to clarify the influences of the explicit solvent water molecules on the vibrational spectra, we have investigated them in aqueous solution, considering the vibrational INM DOS (see eq 4). Figure 4 shows the vibrational INM DOS $\rho(\omega)$ of the glycine molecule in aqueous environment in the high-frequency range (2800−3600 cm^{-1}), where a number of typical stretching modes are observed. Since

dx.doi.org/10.1021/ct500235a | J. Chem. Theory Comput. 2014, 10, 3369−3379

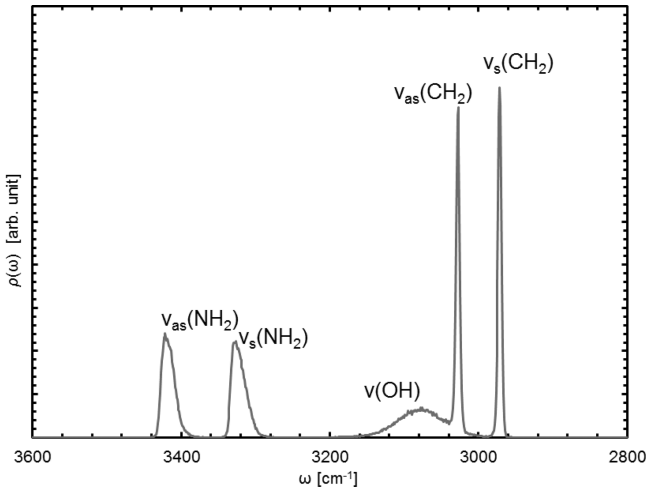

Figure 4. Vibrational INM DOS $\rho(\omega)$ in high-frequency range.

such peak positions agreed with the ω_{FE} values, each peak was appropriately assigned to the corresponding vibrational mode obtained by the VFA-FEH approach (see Table 2). It can be reasonably understood, therefore, that the relatively broad peak in the range of 3000−3160 cm^{-1} should correspond to the stretching motion of the −OH group (3077 cm^{-1}), where its full width at half-maximum (fwhm) is ∼80 cm^{-1}. On the contrary, in the range 3280−3440 cm^{-1}, there were two less broad peaks with each fwhm (∼30 cm^{-1}) less than a half the value of −OH group. Actually, it was found that such two peaks (i.e., 3322 and 3416 cm^{-1}) correspond to the symmetric and the asymmetric modes of $-NH_2$ group, respectively. In contrast to the above three modes, the two modes of $>CH_2$ group (i.e., 3028 and 2972 cm^{-1}) were found to become very sharp since they were hardly influenced electrostatically even in aqueous environment.

Next, we have shown in Figure 5 the approximate IR spectra as the vibrational INM DOS $D^{IR}(\omega)$ (eq 8a) weighed with w_i^{IR} of each vibrational mode (see in parentheses in Table 3). The IR intensities in aqueous solution I_{aq} were found to increase considerably in comparison to those in gas phase I_{gas} with the

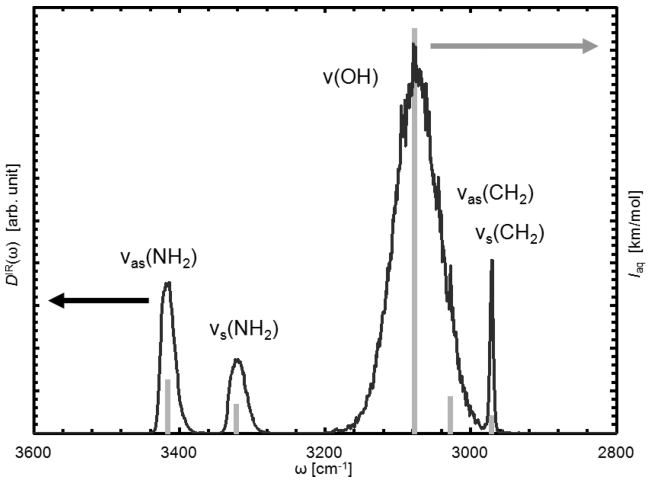

Figure 5. Approximate IR spectra: the vibrational INM DOS $D^{IR}(\omega)$ weighed with w_i^{IR} in high-frequency range. Those average IR intensities I_{aq} at the vibrational frequencies estimated by the VFA-FEH approach are also indicated by the gray bar.

Table 3. Calculated IR Intensities *I* (km/mol) and Shifts from in Gas Phase to in Aqueous Solution Δ*I* (km/mol)

		gas phase	in solution	intensity shift
mode	i	$I_{gas}(\omega_{gas,\,i})$	$I_{aq}(\omega_{FE,\,i})$	ΔI^a
$\nu_{as}(NH_2)$	1	9.9 (3476)	41.7 (3416)	+31.8
$\nu_s(NH_2)$	2	2.9 (3381)	21.9 (3322)	+19.0
ν(OH)	3	73.9 (3570)	331.0 (3077)	+257.1
$\nu_{as}(CH_2)$	4	4.6 (3011)	28.1 (3028)	+23.5
$\nu_s(CH_2)$	5	13.3 (2958)	12.4 (2972)	−0.9
ν(CO)	6	260.6 (1708)	390.3 (1691)	+129.7

$^a\Delta I = I_{aq} - I_{gas}$

exception of that of $\nu_s(CH_2)$ (see Table 3). In particular, since ΔI of the −OH group was the largest among those of all the vibrational modes, the corresponding IR peak showed the maximum in the high-frequency range although the height of $\rho(\omega)$ was the lowest (Figure 4). Thus, it was recognized in the present system that the intrinsic IR intensity of each vibrational mode has a significant influence on the peak height. In addition, it can be said that, in the present VFA methods, the spectroscopic features, for example, peak intensity and broadening of IR spectra, were consistently reproduced with the observation by the common IR spectroscopy measurements.[36−45]

Finally, we have investigated the microscopic origin of the strong broadening of spectra for the −OH group. It should be noted that, since the geometry of the solute molecule was fixed here at the equilibrium structure in aqueous solution, the peak width is influenced clearly by only the fluctuation of electron density that depends on the instantaneous solvent configurations. In particular, such fluctuation should be induced by the HB formation with the closer water molecules around the glycine molecule. Then, we have investigated the correlation between the vibrational spectra and instantaneous configuration of those water molecules. For the purpose, we have focused on the IR spectra of the C═O and O—H stretching modes. Figure 6 shows the scatter plots of the intermolecular HB distances d_{HB} with the nearest-neighboring O (or H) atoms in the water molecule (the left ordinate) and $D^{IR}(\omega)$ (the right ordinate), where the abscissa is taken as the vibrational frequency. In this case, we have also shown the linearly fitted curves, that is, $d_{O—H\cdots O_w} = 0.0031\ \nu(OH) - 7.9532$ and $d_{C=O\cdots H_w} = -0.0249\ \nu(CO) + 43.936$. As a result, ν(OH) was positively correlated with the O—H···O_w distance $d_{O—H\cdots O_w}$, with its correlation coefficient $R = 0.901$, indicating the strong correlation. This positive correlation indicates that ν(OH) is red-shifted as the O—H···O_w distance becomes smaller, which is ascribed to the weakening of O—H bond due to the decrease of the electron density of O—H bond induced by the negative point-charge on the O atom of a closer water molecule. On the other hand, the slope of the fitted curve for ν(CO) became negative, showing relatively weak correlation ($R = -0.623$). Contrary to an above tendency of the O—H group, ν(CO) is blue-shifted as the intermolecular HB distance (the C═O···H_w distance $d_{C=O\cdots H_w}$) becomes smaller. The electron densities in the C═O σ and π bonding orbitals increase slightly due to the polarization but these changes are smaller than the change in the O—H bonding orbital. To interpret and explain this vibrational frequency changes occurring upon HB formation, we performed the natural bond orbital (NBO) analysis in three systems, that is, isolated system and two polarized systems with

dx.doi.org/10.1021/ct500235a | J. Chem. Theory Comput. 2014, 10, 3369−3379

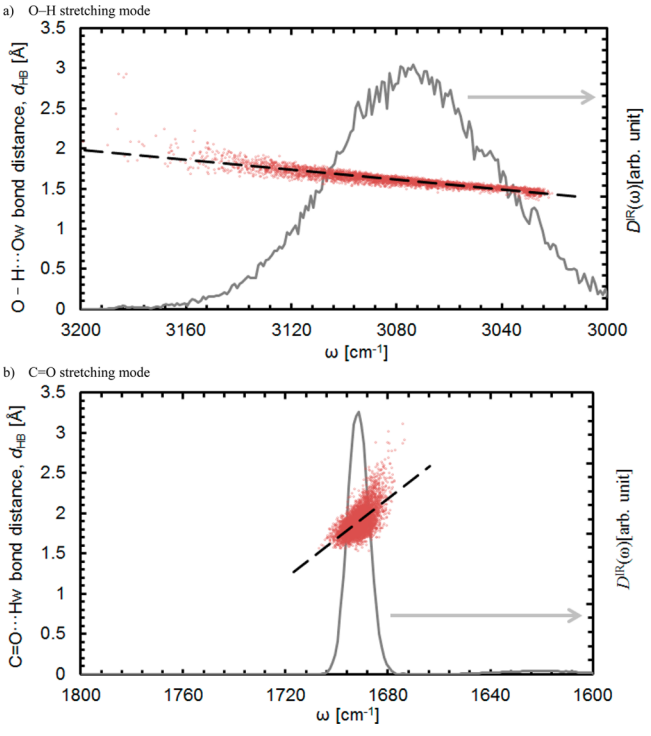

Figure 6. IR spectra of C═O and O—H stretching modes. Scatter plots of the lengths of nearest-neighboring H or O atom of water molecules versus the O—H and C═O stretching frequencies. Linear fits (dashed lines) are (a) $d_{O—H\cdots O_w}$ = 0.0031 ν(OH) − 7.9532; R = 0.901; and (b) $d_{C=O\cdots H_w}$ = −0.0249 ν(CO) + 43.936; R = −0.623.

each point charge (system I and system II). Here, the latter two systems are the simplest HB models polarized with a point-charge expressing the nearest-neighboring atom (O or H). Table 4 shows the hyperconjugative interaction energies $E(2)$ that are estimated by the second order perturbation approach. $E(2)$s in system I scarcely change by the polarization of O—H group. On the contrary, in system II, the LP(O3) → π*(C1—O4) contribution increases due to the polarization of C═O group, giving clear evidence of stabilization originating in the hyperconjugation between lone electron pair of O3 and C═O π* antibonding orbitals. This interaction should bring about the blue-shift of ν(CO). In conclusion, by the polarization, ν(CO) is blue-shifted due to the stabilization by the hyperconjugative interaction, while ν(OH) is red-shifted by the destabilization of the corresponding orbitals.

Table 4. NBO Analysis: Hyperconjugative Interaction Energies Estimated by the Second Order Perturbation Approach $E(2)$ (kcal/mol), and Their Differences between the Isolated System and Two Polarized Systems with Each Point Charge (System I and System II)[a]

	isolated system	system I[c]		system II[d]	
type[b] donor/acceptor	$E(2)$	$E(2)$	Δ	$E(2)$	Δ
LP_1(O3)/BD_1*(C1—O4)	11.12	11.12	0.00	11.14	0.02
LP_2(O3)/BD_2*(C1—O4)	65.5	65.49	−0.01	65.72	0.22
LP_1(O4)/RY_1*(C1)	21.82	21.82	0.00	21.82	0.00
LP_2(O4)/BD_1*(C1—C2)	21.93	21.93	0.00	21.93	0.00
LP_2(O4)/BD_1*(C1—O3)	40.46	40.46	0.00	40.39	−0.07
LP_1(N5)/BD_1*(C1—C2)	12.17	12.17	0.00	12.13	−0.04

[a]The names of atoms in the parentheses and point charges follow those in Figure 3. [b]BD, BD*, RY, and LP mean (σ or π) bonding, (σ* or π*) antibonding, Rydberg, and lone pair AO, respectively. [c]The O—H HB model: A negative point charge (−1e) is located on the position (labeled P1) where is r(H6—P1) = 1.5 Å and θ(O3—H6—P1) = 180°. [d]The C═O HB model: A positive point charge (+1e) is located on the position (labeled P2) where is r(O4—P2) = 1.5 Å and θ(C1—O4—P2) = 150°.

As a result, the vibrational frequencies were found to clearly correlate with the HB distance d_{HB}. Considering that the HB number of −OH group increased in comparison to that of >CO group (see Figure 2), the broadening of IR spectra can be related to the HB strength.

4. CONCLUDING REMARKS

In this study, we have proposed a new theoretical methodology of vibrational spectra in solution, employing two VFAs (vibrational frequency analyses) using analytical Hessians on the FES (FE-Hessian) and instantaneous ones (INM-Hessian) (i.e., VFA-FEH and VFA-INMH). First, we compared the computational performance between analytical and numerical VFA approaches, and confirmed that the present analytical VFA approach is more efficient than the conventional numerical VFA approach. Second, by using the VFA-FEH approach, we investigated the vibrational frequencies and their fluctuations of glycine molecule in aqueous solution under the explicit environment consisting of ambient solvent water molecules. As a result, the calculated vibrational frequencies were quantitatively in good agreement with the experimental ones. For the stretching-mode, the vibrational frequencies of −OH, $-NH_2$ and >CO groups were red-shifted in aqueous solution, while those of $>CH_2$ group were slightly blue-shifted. This is mainly due to the softening (or hardening) of vibrational motions influenced by the structural relaxation in solution, that is, the bond length elongating (or shortening). On the other hand, the bending-modes including −OH and $-NH_2$ groups showed the large blue shifts, being consistent to the experimental observations. This is explained by the hindrance of motion by the adjacent solvent water molecules. Namely, such vibrational shifts are attributed to not only the structural relaxation but also the explicit atomistic solute−solvent interactions.

Third, by using the VFA-INMH approach, we have investigated the approximate IR spectra in solution through the vibrational INM densities of states (DOS). Since such peak positions agreed with the effective vibrational frequencies by the VFA-FEH approach, each peak was appropriately assigned to the corresponding vibrational mode. In particular, since the IR intensity for the —OH group was largest in the high-frequency range, the peak height considerably increased. Namely, such peak heights in the IR spectra must be strongly influenced by the intrinsic IR intensity. Moreover, according to the relationships between the solvent frequency fluctuation and the HB (hydrogen bond) distance, the broadening of IR spectra could be related to the HB strength. In particular, the instantaneous vibrational changes of the —OH group and >CO one can be explained on the basis of two different mechanisms, that is, the change of electron density in OH orbital and hyperconjugation between the lone electron pair of oxygen atom of >CO group and the C═O π* antibonding

dx.doi.org/10.1021/ct500235a | J. Chem. Theory Comput. 2014, 10, 3369−3379

orbital, respectively. This is considered an essential clue to understand the general feature of experimental vibrational spectra in the various HB systems.

In the present study, we have discussed about the IR spectra depending on the electron density induced by the instantaneous solvent configurations, by combining with VFA-FEH approach. However, more realistically, the present method should be executed successively for a set of "instantaneous" structures obtained through an equilibrium (or nonequilibrium) QM/MM-MD trajectory without fixing the structures of solute molecules themselves. Moreover, by using the VFA-INMH approach, any complicated vibrational spectra, which are overlapped by the several vibrational modes, can be, in principle, separated to the contributions of individual vibrational modes. Finally, it is concluded that the present approaches would provide us a plausible tool to analyze vibrational properties separately to the contributions from the original modes and are quite useful to interpret the microscopic origin of the experimental vibrational spectra.

■ ASSOCIATED CONTENT

Supporting Information

Details of the QM/MM-MD and the FEG method to obtain the equilibrium structure in aqueous solution, and the additional results, that is, the equilibrium structure changes in solution and the solvation structure around glycine molecule. This material is available free of charge via the Internet at http://pubs.acs.org.

■ AUTHOR INFORMATION

Corresponding Author

*Tel/Fax: +81-52-789-5623. Email: mnagaoka@is.nagoya-u.ac.jp.

Notes

The authors declare no competing financial interest.

■ ACKNOWLEDGMENTS

This work was supported partly by the a Grant-in-Aid for Science Research from the Ministry of Education, Culture, Sport, Science and Technology (MEXT) in Japan and also by Core Research for Evolutional Science and Technology (CREST) "High Performance Computing for Multi-scale and Multi-physics Phenomena" and "Establishment of Molecular Technology to towards the Creation of New Functions" from the Japan Science and Technology Agency (JST). Y.K. also acknowledges the support from Japan Society for the Promotion of Science (JSPS) by the Research Fellowship for Young Scientist.

■ REFERENCES

(1) Yan, B.; Fell, J. B.; Kumaravel, G. *J. Org. Chem.* **1996**, *61*, 7467−7472.
(2) Nibbering, E. T. J.; Fidder, H.; E. Pines, E. *Annu. Rev. Phys. Chem.* **2005**, *56*, 337−367.
(3) Stead, D.; Carbone, G.; O'Brien, P.; Campos, K. R.; Coldham, I.; Sanderson, A. *J. Am. Chem. Soc.* **2010**, *132*, 7260−7261.
(4) Ramaekers, R.; Pajak, J.; Lambie, B.; Maes, G. *J. Chem. Phys.* **2004**, *120*, 4182−4193.
(5) Boeckx, B.; Maes, G. *J. Phys. Chem. B* **2012**, *116*, 11890−11898.
(6) Tomasi, J.; Persico, M. *Chem. Rev.* **1994**, *94*, 2027−2094.
(7) Acevedo, O.; Jorgensen, W. L. *Org. Lett.* **2004**, *6*, 2881−2884.
(8) Acevedo, O.; Jorgensen, W. L. *J. Am. Chem. Soc.* **2006**, *128*, 6141−6146.
(9) Kitamura, Y.; Takenaka, N.; Koyano, Y.; Nagaoka, M. *Chem. Phys. Lett.* **2011**, *514*, 261−266.
(10) Warshel, A.; Levitt, M. *J. Mol. Biol.* **1976**, *103*, 227−249.
(11) Field, M. J.; Bash, P. A.; Karplus, M. *J. Comput. Chem.* **1990**, *11*, 700−733.
(12) Okuyama-Yoshida, N.; Nagaoka, M.; Yamabe, T. *Int. J. Quantum Chem.* **1998**, *70*, 95−103.
(13) Nagaoka, M.; Okuyama-Yoshida, N.; Yamabe, T. *J. Phys. Chem. A* **1998**, *102*, 8202−8208.
(14) Okuyama-Yoshida, N.; Nagaoka, M.; Yamabe, T. *J. Phys. Chem. A* **1998**, *102*, 285−292.
(15) Okuyama-Yoshida, N.; Kataoka, K.; Nagaoka, M.; Yamabe, T. *J. Chem. Phys.* **2000**, *113*, 3519−3524.
(16) Koyano, Y.; Takenaka, N.; Nakagawa, Y.; Nagaoka, M. *Bull. Chem. Soc. Jpn.* **2010**, *83*, 486−494.
(17) Takenaka, N.; Kitamura, Y.; Koyano, Y.; Asada, T.; Nagaoka, M. *Theor. Chem. Acc.* **2011**, *130*, 215−226.
(18) Galván, I. F.; Sánchez, M. L.; Martín, M. E.; Olivares del Valle, F. J.; Aguilar, M. A. *J. Chem. Phys.* **2003**, *118*, 255−263.
(19) Georg, H. C.; Fernandes, T. S.; Canuto, S.; Takenaka, N.; Kitamura, Y.; Nagaoka, M. In *Practical Aspects of Computational Chemistry III*; Leszczynski, J., Shukla, M. K., Eds.; Springer; New York, 2014; pp 231−247.
(20) Oxtoby, D. W.; Levesque, D.; Weis, J.-J. *J. Chem. Phys.* **1978**, *68*, 5528−5533.
(21) Lawrence, C. P.; Skinner, J. L. *J. Chem. Phys.* **2002**, *117*, 8847−8854.
(22) Lawrence, C. P.; Skinner, J. L. *J. Chem. Phys.* **2003**, *118*, 264−272.
(23) Buchner, M.; Ladanyi, B. M.; Stratt, R. M. *J. Chem. Phys.* **1992**, *97*, 8522−8535.
(24) Cho, M.; Fleming, G. R.; Saito, S.; Ohmine, I.; Stratt, R. M. *J. Chem. Phys.* **1994**, *100*, 6672−6683.
(25) Kindt, J. T.; Schmuttenmaer, C. A. *J. Chem. Phys.* **1997**, *106*, 4389−4400.
(26) Melzer, A.; Schella, A.; Schablinski, J.; Block, D.; Piel, A. *Phys. Rev. E* **2013**, *87*, 033107.
(27) Tuñón, I.; Silla, E.; Ruiz-López, M. F. *Chem. Phys. Lett.* **2000**, *321*, 433−437.
(28) Frisch, M. J.; Trucks, G. W.; Schlegel, H. B.; Scuseria, G. E.; Robb, M. A.; Cheeseman, J. R.; Scalmani, G.; Barone, V.; Mennucci, B.; Petersson, G. A.; Nakatsuji, H.; Caricato, M.; Li, X.; Hratchian, H. P.; Izmaylov, A. F.; Bloino, J.; Zheng, G.; Sonnenberg, J. L.; Hada, M.; Ehara, M.; Toyota, K.; Fukuda, R.; Hasegawa, J.; Ishida, M.; Nakajima, T.; Honda, Y.; Kitao, O.; Nakai, H.; T, V.; Montgomery, J. A., Jr.; Peralta, J. E.; Ogliaro, F.; Bearpark, M.; Heyd, J. J.; Brothers, E.; Kudin, K. N.; Staroverov, V. N.; Kobayashi, R.; Normand, J.; Raghavachari, K.; Rendell, A.; Burant, J. C.; Iyengar, S. S.; Tomasi, J.; Cossi, M.; Rega, N.; Millam, J. M.; Klene, M.; Knox, J. E.; Cross, J. B.; Bakken, V.; Adamo, C.; Jaramillo, J.; Gomperts, R.; Stratmann, R. E.; Yazyev, O.; Austin, A. J.; Cammi, R.; Pomelli, C.; Ochterski, J. W.; Martin, R. L.; Morokuma, K.; Zakrzewski, V. G.; Voth, G. A.; Salvador, P.; Dannenberg, J. J.; Dapprich, S.; Daniels, A. D.; Farkas, O.; Foresman, J. B.; Ortiz, J. V.; Cioslowski, J.; Fox, D. J. *Gaussian 09, Revision A.02*; Gaussian Inc.: Wallingford, CT, 2009.
(29) Singh, U. C.; Kollman, P. A. *J. Comput. Chem.* **1984**, *5*, 129−145.
(30) Besler, B. H.; Merz, K. M., Jr.; Kollman, P. A. *J. Comput. Chem.* **1990**, *11*, 431−439.
(31) Okamoto, T.; Yamada, K.; Koyano, Y.; Asada, T.; Koga, N.; Nagaoka, M. *J. Comput. Chem.* **2010**, *32*, 932−942.
(32) Case, D. A.; Darden, T. A.; Cheatham, T. E.; Simmerling, C. L.; Wang, J.; Duke, R. E.; Luo, R.; Merz, K. M., Jr.; Pearlman, D. A.; Crowley, M.; Walker, R. C.; Zhang, W.; Wang, B.; Hayik, S.; Roitberg, A. E.; Seabra, G.; Wong, K. F.; Paesani, F.; Wu, X.; Brozell, S.; Tsui, V.; Gohlke, H.; Yang, L.; Tan, C.; Mongan, J.; Hornak, V.; Cui, G.; Beroza, P.; Mathews, D. H.; Schafmeister, C. E. A. F.; Ross, W. S.; Kollman, P. A. *AMBER 9*; University of California: San Francisco, 2006.

(33) Frisch, M. J; Trucks, G. W.; Schlegel, H. B.; Scuseria, G. E.; Robb, M. A.; Cheeseman, J. R.; Montgomery, Jr., J. A.; Vreven, T.; Kudin, K. N.; Burant, J. C.; Millam, J. M.; Iyengar, S. S.; Tomasi, J.; Barone, V.; Mennucci, B.; Cossi, M.; Scalmani, G.; Rega, N.; Petersson, G. A.; Nakatsuji, H.; Hada, M.; Ehara, M.; Toyota, K.; Fukuda, R.; Hasegawa, J.; Ishida, M.; Nakajima, T.; Honda, Y.; Kitao, O.; Nakai, H.; Klene, M.; Li, X.; Knox, J. E.; Hratchian, H. P.; Cross, J. B.; Bakken, V.; Adamo, C.; Jaramillo, J.; Gomperts, R.; Stratmann, R. E.; Yazyev, O.; Austin, A. J.; Cammi, R.; Pomelli, C.; Ochterski, J. W.; Ayala, P. Y.; Morokuma, K.; Voth, G. A.; Salvador, P.; Dannenberg, J. J.; Zakrzewski, V. G.; Dapprich, S.; Daniels, A. D.; Strain, M. C.; Farkas, O.; Malick, D. K.; Rabuck, A. D.; Raghavachari, K.; Foresman, J. B.; Ortiz, J. V.; Cui, Q.; Baboul, A. G.; Clifford, S.; Cioslowski, J.; Stefanov, B. B.; Liu, G.; Liashenko, A.; Piskorz, P.; Komaromi, I.; Martin, R. L.; Fox, D. J.; Keith, T.; Al-Laham, M. A.; Peng, C. Y.; Nanayakkara, A.; Challacombe, M.; Gill, P. M. W.; Johnson, B.; Chen, W.; Wong, M. W.; Gonzalez, C.; Pople, J. A. *Gaussian 03, Revision C.02*; Gaussian, Inc.: Wallingford, CT, 2004.
(34) Jorgensen, W. L.; Chandrasekhar, J.; Madura, J. D. *J. Chem. Phys.* **1983**, *79*, 926−935.
(35) Merrick, J. P.; Moran, D.; Radom, L. *J. Phys. Chem. A* **2007**, *111*, 11683−11700.
(36) Badger, R. M.; Bauer, S. H. *J. Chem. Phys.* **1937**, *5*, 839−851.
(37) Badger, R. M. *J. Chem. Phys.* **1940**, *8*, 288−289.
(38) Huggins, C. M.; Pimentel, G. C. *J. Phys. Chem.* **1956**, *60*, 1615−1619.
(39) Allerhand, A.; von R. Schleyer, P. *J. Am. Chem. Soc.* **1963**, *85*, 371−380.
(40) Drago, R. S.; O'Bryan, N.; Vogel, G. C. *J. Am. Chem. Soc.* **1970**, *92*, 3924−3929.
(41) Mizuno, K.; Miyashita, Y.; Shindo, Y.; Ogawa, H. *J. Phys. Chem.* **1995**, *99*, 3225−3228.
(42) Freda, M.; Onori, G.; Santucci, A. *J. Phys. Chem. B* **2001**, *105*, 12714−12718.
(43) Tanabe, S.; Ebata, T.; Fujii, M.; Mikami, N. *Chem. Phys. Lett.* **1993**, *215*, 347−352.
(44) Kubelka, J.; Keiderling, T. A. *J. Phys. Chem. A* **2001**, *105*, 10922−10928.
(45) Jansen, T. L.; Knoester, J. *J. Chem. Phys.* **2006**, *124*, 044502.
(46) Grabowski, S. J. *Chem. Rev.* **2011**, *111*, 2597−2625.
(47) Leung, K.; Rempe, S. B. *J. Chem. Phys.* **2005**, *122*, 184506.
(48) Handy, N. C.; Amos, R. D.; Gaw, J. F.; Rice, J. E.; Simandiras, E. D. *Chem. Phys. Lett.* **1985**, *120*, 151−158.
(49) Harrison, R. J.; Fitzgerald, G. B.; Laidig, W. D.; Bartlett, R. J. *Chem. Phys. Lett.* **1986**, *124*, 291−294.